The Dynamic Distribution of Fluorescent Analogues of Actin and Myosin in Protrusions at the Leading Edge of Migrating Swiss 3T3 Fibroblasts

Robbin L. DeBiasio, Lei-Lei Wang, Gregory W. Fisher, and D. Lansing Taylor

Department of Biological Sciences and Center for Fluorescence Research in Biomedical Sciences, Carnegie Mellon University, Pittsburgh, Pennsylvania 15213

Abstract. The formation of protrusions at the leading edge of the cell is an essential step in fibroblast locomotion. Using fluorescent analogue cytochemistry, ratio imaging, multiple parameter analysis, and fluorescence photobleaching recovery, the distribution of actin and myosin was examined in the same protrusions at the leading edge of live, locomoting cells during wound-healing in vitro. We have previously defined two temporal stages of the formation of protrusions: (*a*) initial protrusion and (*b*) established protrusion (Fisher et al., 1988). Actin was slightly concentrated in initial protrusions, while myosin was either totally absent or present at extremely low levels at the base of the initial protrusions. In contrast, established protrusions contained diffuse actin and actin microspikes, as well as myosin in both diffuse and structured forms. Actin and myosin were also localized along concave transverse fibers near the base of initial and established protrusions. The dynamics of myosin penetration into a relatively stable, established protrusion was demonstrated by recording sequential images over time. Myosin was shown to be absent from an initial protrusion, but diffuse and punctate myosin was detected in the same protrusion within 1–2 min. Fluorescence photobleaching recovery indicated that myosin was 100% immobile in the region behind the leading edge containing transverse fibers, in comparison to the 21% immobile fraction detected in the perinuclear region. Possible explanations of the delayed penetration of myosin into established protrusions and the implications on the mechanism of protrusion are discussed.

FIBROBLAST cell movement must involve a complex sequence of mechano-chemical steps leading to localized protrusive activity at the leading edge, adherence of the protrusion to the substrate and cell translocation (Trinkaus, 1985; Singer and Kupfer, 1986). There is currently no universally accepted mechanism of fibroblast locomotion, but protrusions at the leading edge of migrating cells are generally believed to play a fundamental role in the process. Therefore, one important step toward an understanding of the molecular basis of fibroblast locomotion is the determination of the mechanism of protrusion at the leading edge of migrating cells.

Knowledge of the distribution of the major cytoskeletal and contractile proteins in and near protrusions could facilitate the understanding of the forces responsible for protrusions. Previous studies using immunofluorescence have demonstrated that cell protrusions contain actin (Mooseker and Tilney, 1975; Herman et al., 1981; Gotlieb et al., 1979; Small, 1981), vinculin and talin (David-Pfeuty, 1985; Geiger et al., 1984), α-actinin (Geiger et al., 1984), and filamin (Geiger et al., 1984; Heggeness et al., 1977). The presence of these components in cell protrusions suggests that substrate attachment proteins, actin, and actin-binding proteins can participate in the protrusive activity of nonmuscle cells. It has been reported that protrusions in fibroblasts lack intermediate filaments (Kolega, 1985) and microtubules (Letourneau, 1985), and contain very little or no standard myosin (myosin II; Herman et al., 1981; Willingham et al., 1981; Singer and Kupfer, 1986; Heggeness et al., 1977). A recent immunofluorescence study indicates that both microtubules and myosin II can penetrate into protrusions in a time dependent manner during wound healing in vitro (Conrad, P., A. Waggoner, I. Herman, M. Nederlof, and D. Taylor, manuscript in preparation). Unfortunately, the relative distribution of selected cytoskeletal and contractile proteins have been based on the qualitative comparisons of separate immunofluorescence images of fixed cells. Therefore, only qualitative and static structural information have been obtained.

It is now possible to define temporal and spatial changes in the distribution and mobility of selected molecules in living cells using fluorescent analogue cytochemistry (Taylor and Wang, 1978; see Taylor et al., 1986 for a review), ratio imaging (Tanasugarn et al., 1984; Bright et al., 1987; Luby-

Phelps and Taylor, 1988), multiple parameter analysis (DeBiasio et al., 1987), and fluorescence photobleaching recovery (Wang et al., 1982; Kreis et al., 1982; Amato and Taylor, 1986; Wang, 1985). The present study concerns the distribution of actin and myosin in migrating fibroblasts during wound healing in vitro to relate the distribution of actin and myosin to protrusive activity at the leading edge. We have found that subcellular components within the protrusion during initial extension of the membrane differ from components within the same protrusive region at a later time.

Materials and Methods

Cell Culture and Preparation

Swiss 3T3 fibroblast cells (CCL92; American Type Culture Collection, Rockville, MD) were maintained in phenol red-free DME (Gibco Laboratories, Grand Island, NY), pH 7.4, containing 2 mg/ml penicillin, 0.05 mg/ml streptomycin, and 10% calf serum (complete DME [c-DME][1]). Subconfluent 3T3 cells were subcultured every 3 d by trypsinization using 0.05% trypsin and 0.02% EDTA in a Ca-Mg-free saline solution (Gibco Laboratories). All cell cultures were incubated in a humidified, 5% CO_2 environment at 37°C. Cell passage number ranged from 122 to 126.

To obtain well-spread single cells on 40 mm round glass coverslips (Bellco Glass Inc., Vineland, NJ), $\sim 2 \times 10^4$ 3T3 cells in c-DME were seeded on coverslips in 60-mm culture dishes (Corning Glass Works, Corning, NY). Subconfluent coverslips were used 3 d after plating.

To obtain confluent monolayers of 3T3 cells on 40-mm round glass coverslips, $\sim 2.5 \times 10^5$ 3T3 cells in c-DME were seeded on coverslips in 60-mm culture dishes. Confluent monolayers on coverslips were obtained in 2 d. Coverslips were used in the wound-healing studies on the third day, after monolayers had been confluent for 24 h.

Polarized 3T3 cells were generated by wounding a confluent monolayer (Todaro et al., 1967). A ~2-mm wide slash was made through the cell sheet using a dull edged razor blade. Cell aggregates along the wound were removed leaving a straight wound edge which decreased multidirectional migration and enhanced uniform forward movement. The coverslips were rinsed with c-DME to remove cell debris and incubated at 37°C, 5% CO_2 for a minimum of 20 min before microinjection.

Video-enhanced Contrast Microscopy

Wounded monolayers of 3T3 cells on coverslips were mounted in Dvorak-Stotler chambers (Nicholson Precision Instruments, Inc., Gaithersburg, MD) with 18-h equilibrated c-DMEM. The temperature (37°C) was maintained by a thermistor placed against the coverslip containing cells, which was connected to a microcomputer controlled modified air curtain (Bright et al., 1987).

Cells were observed using a Zeiss Photomicroscope III, a Zeiss 100× plan apo, 1.25 NA objective, with the optovar setting of 2.0 and Nomarski differential interference contrast optics. A chalnicon camera (Hamamatsu Corp., Middlesex, NJ) and a microscope system image processor (Phototonic Microscopy, Inc., Oak Brook, IL) were set in the video-enhanced contrast (VEC) mode with two frame mottle subtract and rolling average. Images were stored on tape using a video casette recorder (model NV-9240 XD; Panasonic, New York, NY).

Cells were examined ~2 h after wounding. Cellular substructures within protrusions were observed over a period of several minutes. VEC images at selected time points were photographed from the monitor (Hamamatsu Corp.).

Fluorescent Volume Indicator

A fluorescent, low molecular weight volume indicator capable of penetrating into the peripheral regions of the cell allowed us to observe the thin initial protrusions at the leading edge of migrating cells and to normalize the actin or myosin images for changes in pathlength throughout the cell (see Image Processing below). Dimethylfluorescein-dextran, molecular weight 5,000 (FL-dextran-5K) obtained through the courtesy of Dr. Luis Glaser, was coinjected with the fluorescent analogues of actin or smooth muscle myosin.

Fluorescent Actin Analogue

Actin was purified from rabbit back muscles (Spudich and Watt, 1971), and labeled with 5-iodoacetamidofluorescein (AF-actin; Molecular Probes, Inc., Junction City, OR) as previously described (Wang and Taylor, 1980) or with 5-tetramethylrhodamine-5 (and -6) iodoacetamide (AR-actin; Molecular Probes, Inc.) (Taylor et al., 1981; Tait and Frieden, 1982; Simon et al., 1988). Final AF-actin and AR-actin preparations were prepared in an injection buffer solution of 2 mM Pipes, 0.1 mM ATP, 0.1 mm dithrothreitol (DTT), 0.05 mM $MgCl_2$, pH 7.0 (25°C). Optimal incorporation and fluorescence levels were achieved by using a stock-labeled actin at a concentration of ~4 mg/ml with a dye to protein ratio of 1.0. The volume of actin solution microinjected ranged from 2 to 5% of total cell volume (Amato and Taylor, 1986).

Fluorescent Myosin Analogue

Smooth muscle myosin was purified from either frozen or fresh chicken gizzards (supplied by Pel-Freeze Biologicals, Rogers, AR; or Joey's Poultry and Fish, Pittsburgh, PA) using the procedure described by Sellers et al. (1981) and Sobieszek and Bremel (1975), with minor modifications. Isolated myosin was >95% pure as indicated by SDS-PAGE (Laemmli, 1970). Myosin was used immediately for the preparation of the fluorescent analogue, or was stored on ice for up to 6 wk in storage buffer, (10 mM 3-[N-morpholino] propanesulfonic acid [MOPS], 50 mM NaCl, 0.1 mM EGTA, 0.1 mM $MgCl_2$, 1.0 mM DTT, 0.2 mM PMSF, and 0.02% sodium azide, pH 7.0, 4°C). Fluorescent dyes, 5-tetramethylrhodamine-5 (and -6) iodoacetamide (IAR) or 5-iodoacetamidofluorescein (IAF), (Molecular Probes Inc.), were used for fluorescent myosin preparation. All procedures were carried out at a temperature between 0 and 4°C, unless otherwise specified.

2 ml of myosin (>10 mg/ml) in storage buffer was precipitated by adding 10 mM $MgCl_2$. After 15 min on ice, the myosin was centrifuged in an Eppendorf centrifuge (model 5415; Brinkmann Instruments Co., Westbury, NY) for 10 min at 8,000 *g*. The myosin pellet was resuspended into 1 ml labeling buffer I (10 mM Hepes, 50 mM KCl, 0.2 mM EGTA, pH 7.0) and dialyzed against 500 ml of the same buffer for 2 h in a 25,000-mol wt cutoff collodion bag (Schleicher & Schull Inc., Keene, NH). The concentration of myosin (mg/ml) was determined either by the method of Bradford (1976) using BSA as a standard, or spectrophotometrically using an extinction coefficient $E_{280}^{0.1\%} = 0.52$ cm^{-1} (Sellers and Pato, 1984). The rest of the myosin was diluted as necessary to a concentration of 12–15 mg/ml with labeling buffer I and then dialyzed for 2 h against 500 ml labeling buffer II (10 mM HEPES, 50 mM KCl, 0.2 mM EGTA, 2 mM ATP, 2 mM $MgCl_2$, pH 7.0). The turbid myosin solution became clear as the ATP concentration inside the collodion bag increased. After the removal of myosin from the collodion bag, the volume of the solution was measured and the molar concentration was calculated using a molecular weight of 460,000. IAF or IAR was dissolved into dimethylformamide to a concentration of 40 mM. A 10-fold molar excess of IAF or IAR was added slowly to the myosin solution. The mixture was then incubated on ice overnight in the dark. The labeling reaction was quenched by the addition of 2 mM DTT. Labeled myosin was dialyzed against 500 ml labeling buffer I for 3 h in a collodion bag. The myosin solution was collected and $MgCl_2$ was added to achieve a final concentration of 10 mM. The myosin was centrifuged again in an Eppendorf centrifuge (Brinkman Instruments Co.) for 10 min at 8,000 *g*. Pellets of IAF-labeled myosin (AF-myosin) or the IAR-labeled myosin (AR-myosin) were resuspended and dialyzed overnight against 1 liter of buffer H (2 mM Hepes, 0.1, mM EGTA, 1.0 mM DTT, pH 7.5). The fluorophores were covalently linked to the myosin and there was no detectable free dye, as indicated by SDS-PAGE. The fluorescent analogues had a dye/protein ratio of ~6. The extinction coefficients (determined in 10 mM Hepes, 0.5 M KCl, pH 7.0, 25°C) were $E_{495}^{M} = 6.6 \times 10^4$ for IAF; and $E_{552}^{M} = 4.7 \times 10^4$ for IAR. The fluorescence intensity on a SDS polyacrylamide gel indicated that the myosin heavy chain had approximately twice the labeling as the 17-kD myosin light chain.

Immediately before microinjection, the solution of labeled myosin in buffer H was adjusted to achieve a final concentration of 0.2 mM $MgCl_2$, 0.2 mM ATP (pH 7.0), and 100 mM NaCl, at 0°C. The labeled myosin solution was clarified by centrifugation for 5 min at 76,500 *g* in a Beckman Airfuge (Beckman Instruments Inc., Palo Alto, CA). The supernatant was col-

1. *Abbreviations used in this paper*: c-DME, complete DME; IAF, 5-iodoacetamidofluorescein; IAR, tetramethylrhodamine-5 (and -6) iodoacetamide; VEC, video-enhanced contrast.

lected and used for microinjection. The myosin concentration in the supernatant was ~5 mg/ml.

Characterization of the Fluorescent Myosin Analogues. Both AF-myosin and AR-myosin are capable of assembling into thick filaments that could be solubilized with the addition of Mg-ATP. The critical concentration of native purified myosin and AR-myosin was 2 μg/ml and 4 μg/ml, respectively, in buffer containing 10 mM MOPS, 0.1 M KCl, 2 mM $MgCl_2$, 0.1 mM DTT, 0.5 mM EGTA, pH 7.0, at 4°C.

In addition, both AR-myosin and AF-myosin could be phosphorylated by chicken gizzard myosin light-chain kinase, purified according to the procedure of Ngai et al. (1984). Phosphorylated AR-myosin has an actin-activated Mg-ATPase activity of 29.6 nmol/min per mg compared to 30.1 nmol/min per mg for native myosin assayed under similar conditions as described by Seller et al. (1981). Details of the biochemical and spectroscopic characterization of the fluorescent myosin analogue will be published elsewhere.

Cell Labeling Procedure

Single Cell Studies. Well-spread 3T3 cells from subconfluent cultures were microinjected (Amato et al., 1983) with AF-myosin in the presence of c-DME and incubated for 2 h at 37°C, 5% CO_2, before imaging and photobleaching.

Wound-healing Studies. Migrating cells along both edges of the 2-mm-wide wound were microinjected with either (*a*) a mixture of AF-actin (4 mg/ml) and the volume indicator FL-dextran-5K (5 mg/ml), or (*b*) a mixture of AR-myosin (5 mg/ml) and FL-dextran-5K (5 mg/ml). The third set of experiments examining the distribution of actin and myosin in the same living cell required a double injection procedure. The cells were microinjected first with AF-actin, and after a 1.5-h incubation period, the same cells were microinjected with AR-myosin. For photobleaching studies, migrating cells along the wound edge were microinjected with AF-myosin. All microinjected cells were incubated for 1.5 h before imaging.

Coverslips were rinsed and mounted in modified Sykes-Moore chambers (Bellco Glass Inc.; Bright et al., 1987) using c-DME which had been equilibrated for a minimum of 18 h in a 37°C, 5% CO_2 incubator. Labeled cells were examined 2.5–4.0 h after wounding.

Fluorescence Photobleaching Recovery

Migrating 3T3 cells were microinjected with AF-myosin, and 3 h after wounding, selected regions around the nucleus and at the leading edge were photobleached with a 6-μm radius laser spot and the fluorescence recovery was monitored periodically over 60 s after bleaching using the equipment and methods described previously (Luby-Phelps et al., 1985, 1986, 1987).

Digital Imaging Microscopy

The microscope imaging system used to acquire, process, and display the images has been previously described in detail (Bright et al., 1987; DeBiasio et al., 1987). The system included a Universal microscope stand (Carl Zeiss, Inc., Thornwood, NY), a scanning stage (Carl Zeiss, Inc.), an intensified silicon-intensified target camera (model No. 66; Dage-MTI, Inc., Wabash, MI) and an image processor (Vicom Systems, Inc., San Jose, CA). Some data analysis and display were performed on the BioVision microscope workstation (Perceptics Corp., Knoxville, TN).

The excitation light was generated from a 12-V tungsten-halogen filament lamp, operated at a constant current of 7.7 A. The intensifier was operated at 7,000 V and the gain was adjusted to 20% of the maximum setting. All experiments used a 63× water immersion Plan-Neofluor objective (1.2 NA; Carl Zeiss, Inc.). Fluorescein (ex 490 nm, em 520 nm) and rhodamine (ex 570 nm, em 590 nm) filter sets were employed (DeBiasio et al., 1987).

A custom heating stage (Ranin Instruments Co. Inc., Woburn, MA) which surrounded the sealed Sykes-Moore chamber, provided the primary temperature control. A thermistor threaded through a needle port in the chamber, maintained the internal chamber temperature to 37.0°C (± 0.2°C) via a custom microprocessor feedback controlled air curtain (Bright et al., 1987).

Image Acquisition

Myosin Analogue Incorporation. Sets of images (image, background) were acquired sequentially for individual cells injected with AF-myosin.

Wound-healing Studies. Images were acquired in rapid succession using 128 frame integration. Five images were acquired sequentially in the following order: (*a*) volume indicator, (*b*) actin (or myosin), (*c*) volume indicator, (*d*) volume indicator background, and (*e*) actin (or myosin) background. In experiments studying the distribution of actin and myosin in the same cell, the sequence was (*a*) actin, (*b*) myosin, (*c*) actin, (*d*) actin background, and (*e*) myosin background. The second volume image (or the second actin image in the double injection experiments) verified the position of the protrusion after acquisition of the second image. Therefore, an absence or decrease in fluorescence within the protrusion was not due to retraction of the protrusion after the first image was acquired. Only those image sets where little or no motion was detected between the first and second images of the volume indicator were used for further analyses.

Image Processing

Ratio Images. Fluorescence ratio imaging provides a means of examining the temporal and spatial dynamics of labeled molecules within living cells (Tanasugarn et al., 1984; Bright et al., 1987). The thickness of the cytoplasm and the position and density of labeled cellular components vary within the cell, and the fluorescence signal from a cell is proportional to the thickness and accessible volume as well as the concentration of the probe. Ratio imaging normalizes for the differences in pathlength and accessible volume. Background subtracted images were superimposed, the region of interest in both images was masked, and the pixel values within the mask were divided by the pixel values of the same region of interest in the second image.

The actin (or myosin) image was normalized by dividing by the first volume indicator image to produce the actin (or myosin) ratio images. The second volume image was divided by the first volume image to demonstrate the degree of cell movement between the first image and the volume image acquired after the actin (or myosin) image. Higher gray scale values indicated areas of elevated actin (or myosin) concentration relative to the volume indicator. Lower gray scale values corresponded to lower relative concentrations of actin (or myosin). Areas of similar fluorescence intensity in both images resulted in uniform areas within the ratio image. It should be noted that quantitative determinations of the distribution of cellular components cannot be made without this type of normalization.

Black and White Images. All images were background subtracted and enhanced for display purposes by using a variety of image enhancement techniques including histogram stretching, thresholding, and unsharp masking (Castleman, 1979).

Color Composite Images. Red and green images were generated by displaying the volume image in the red channel and the actin (or myosin) in the green channel. Simultaneous display of red and green inputs resulted in images with areas of yellow shading in cell regions where the actin or myosin (green channel) and the volume indicator (red channel) occupied similar areas with similar intensities. In the double injection experiments, the actin image was displayed in the red channel and the myosin image in the green channel.

Results

Smooth Muscle Myosin Analogue Incorporation

Fig. 1 demonstrates the incorporation of the smooth muscle myosin analogue (AF-myosin) in Swiss 3T3 fibroblasts. Single, well-spread, relatively nonmotile 3T3 cells (Fig. 1 *a*) displayed myosin incorporation into numerous stress fibers throughout the cell. Diffuse perinuclear fluorescence was observed and a fine myosin network was also present throughout most of the cell. Fig. 1 *b* demonstrates the punctate and periodic distribution of myosin along stress fibers in part of a large, well-spread, nonmotile 3T3 cell. Most of the labeled myosin was detected in stress fibers. The image processing technique of unsharp masking enhanced the detection of the periodic distribution of labeled myosin along the fibers. In contrast, unsharp masking performed on images of cells containing stress fibers with labeled actin did not reveal a dramatic punctate fluorescence pattern (data not shown). The myosin analogue in 3T3 cells examined 3 h after wounding was found in transverse fibers arranged perpendicular to the direction of migration in both the leading edge and in the

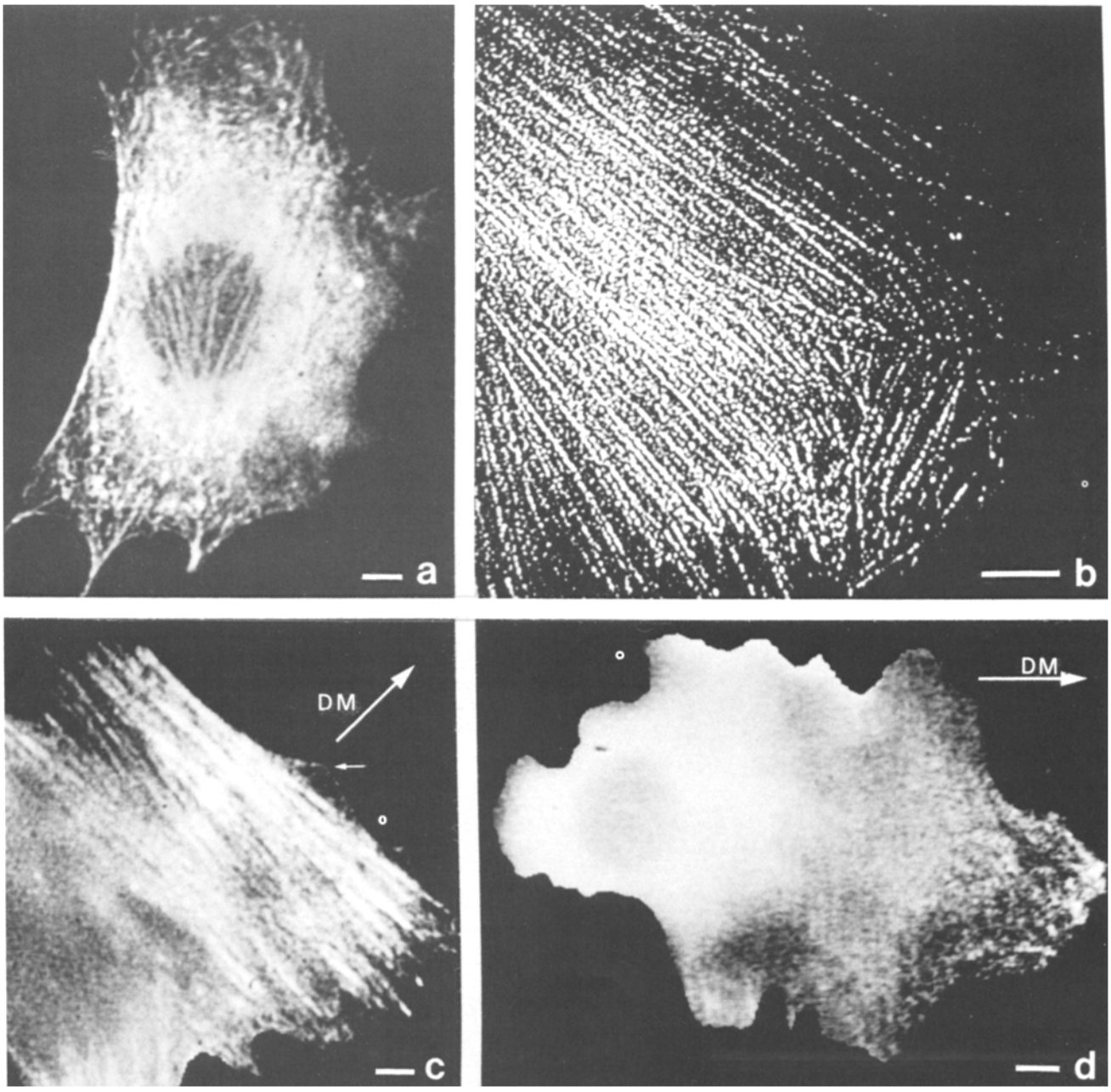

Figure 1. Smooth muscle myosin analogue (AF-myosin) incorporation after microinjection into 3T3 fibroblasts. (*a*) The distribution of myosin in a single, relatively nonmotile cell. (*b*) The periodic and punctate distribution of myosin along fibers in part of a very large, well-spread, nonmotile 3T3 cell. (*c*) 3 h after wounding, myosin was present in transverse fibers arranged perpendicular to the direction of cell migration, and diffuse myosin fluorescence was observed predominately around the nucleus. Myosin was detected in a protrusion at the leading edge (*small arrow*). (*d*) 8 h after wounding, locomoting 3T3 cells displayed a more uniform meshwork of myosin with diffuse myosin fluorescence throughout the cell. Very few stress fibers were observed in elongated locomoting cells. *DM*, direction of migration. Bars, 7 μm.

extending lamellum (Fig. 1 *c*). Myosin in the transverse fibers often exhibited a periodic and punctate pattern. Diffuse myosin fluorescence was observed throughout the cell (excluding initial protrusions, see below), with the larger fraction of diffuse myosin located around the nucleus. Cells in the confluent monolayer, before wounding, and cells located at a distance behind the cells along the wound edge, did not exhibit a unipolar distribution of numerous transverse actin and myosin-containing fibers. After fibroblasts along the wound edge began directional locomotion, the cells behind these migrating cells often contained transverse fibers located on the side of the cell closest to the wound. 8 h after wounding (Fig. 1 *d*), translocating 3T3 cells were elongated, contained very few well-defined stress fibers and transverse fibers, and displayed a more uniform meshwork of myosin fluorescence throughout the cell.

Dynamics of Initial and Established Protrusions: VEC Microscopy

Early protrusive activity has been divided into two defined temporal stages called initial protrusions and established protrusions (Fisher et al., 1988). An initial protrusion is described as a highly flattened, thin membrane sheet that spreads parallel to the substrate, producing a smooth edged, semi-circular protrusion at the front edge of a migrating fibroblast. These protrusions occurred over several seconds or occasionally several minutes. When the forward extension of the initial protrusion ceased, the protrusion was considered an established protrusion, and subsequent movements were considered events of established protrusions. Stationary established protrusions were primarily used in this study since they enabled us to investigate the distribution of actin and myosin in fibroblast protrusions, independent of forward extension, ruffling, or retraction. Subclassifications of protrusions were used in this study to reflect the temporal sequence of protrusive activities and to correlate the presence, absence, or mobilization of cytoskeletal/contractile components with the stage and activity of the protrusion.

VEC miroscopy of the dynamics of initial and established protrusions along the leading edge of SW3T3 cells was demonstrated in Fig. 2. Initial protrusions (*open arrow*) did not contain well-defined subcellular structures. Macromolecular changes within the relatively stable protrusion were detected over time. Within ~1 min after the forward extension of the initial protrusion ceased, small microspikes (Fig. 2 *b*, *small arrows*) were detected in the established protrusion. After an additional minute, well-defined microspikes (Fig. 2 *c*, *small arrows*), extended from the anterior edge of the protrusion to the region of the transverse fibers at the base of the protrusion. Transverse fibers and microspikes observed by VEC microscopy have been shown to be actin-containing structures (Fisher et al., 1988). The study of the dynamics of protrusions by VEC microscopy has provided baseline information on the temporal appearance of cytoskeletal components during defined stages of the formation of protrusions.

Distribution of Actin in Initial Protrusions

The first volume image (Fig. 3 *a*) depicts two initial protrusions (*white arrows*) along the front edge of the same cell. The actin image (Fig. 3 *b*) demonstrated the presence of diffuse fluorescence throughout both of the initial protrusions (*white arrows*), the boundaries of which were defined with the volume image (Fig. 3 *a*). Initial protrusions were much larger in cells that displayed fibers at the base of the protrusions arranged perpendicular to the direction of migration. A two-color composite image of Fig. 3 *a* and *b* is displayed in Fig. 4 *a*.

FL-dextran-5K was selected as the soluble volume indicator since it penetrates into the thin initial protrusions and does not appear to bind to cytoplasmic components (Luby-Phelps et al., 1985). It therefore defines the volume of the cell. We have not yet detected any substantial variations of pH in protrusions (Bright and Taylor, unpublished observations) and the pH of the cytoplasm in these cells is ~pH 7.35 (Bright et al., 1987). Therefore, the pH sensitivity of FL-dextran-5K should not be a factor in these experiments (Bright and Taylor, unpublished observations). The actin ratio image (Fig. 3 *d*) normalized the actin image by correcting for pathlength changes throughout the cell. The actin analogue (and the myosin analogue in the experiments described below) became concentrated in specific domains within the cell. A scan line (Fig. 3 *f*) through the actin/volume ratio image

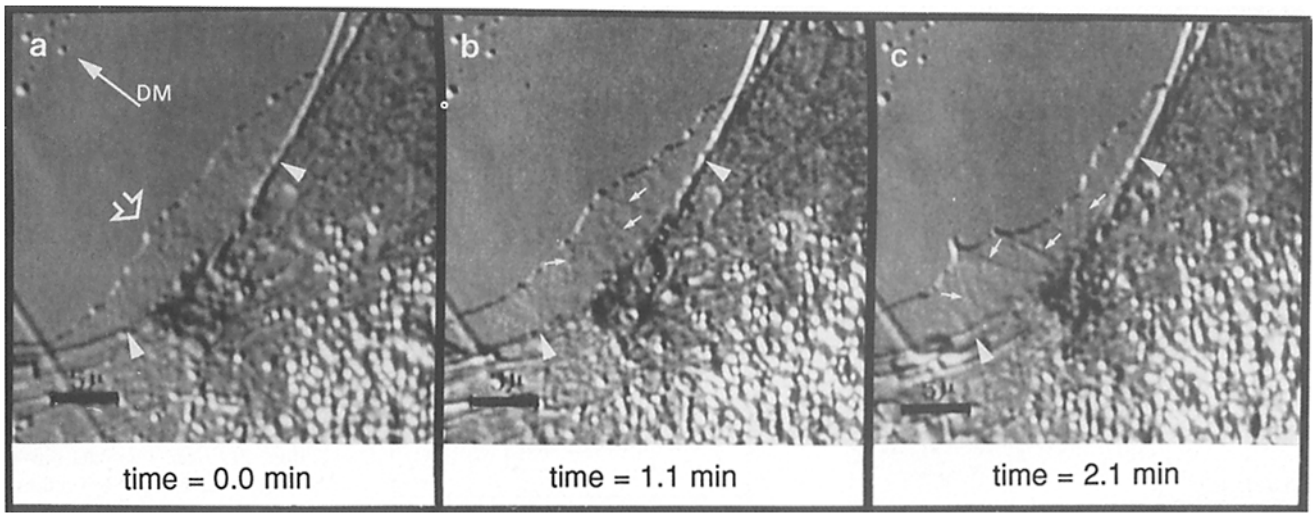

Figure 2. Dynamics of initial and established protrusions using VEC microscopy. 2 h after wounding, the formation of initial protrusions was observed, and the subcellular changes within the protrusion were recorded over a period of several minutes. (*a*) An initial protrusion (*open arrow*) was observed spreading uniformly along the substrate. Well-defined structures were not detected within the initial protrusion, yet concave, transverse fibers (*arrowheads*), were detected at the base of the protrusion. (*b*) Approximately 1 min later, numerous thin fibers (*small arrows*) were observed within the protrusion. (*c*) After an additional minute, well-defined fibers (*small arrows*) extended from the leading edge of the protrusion to a region near the transverse fibers at the base of the protrusion. *DM*, direction of migration.

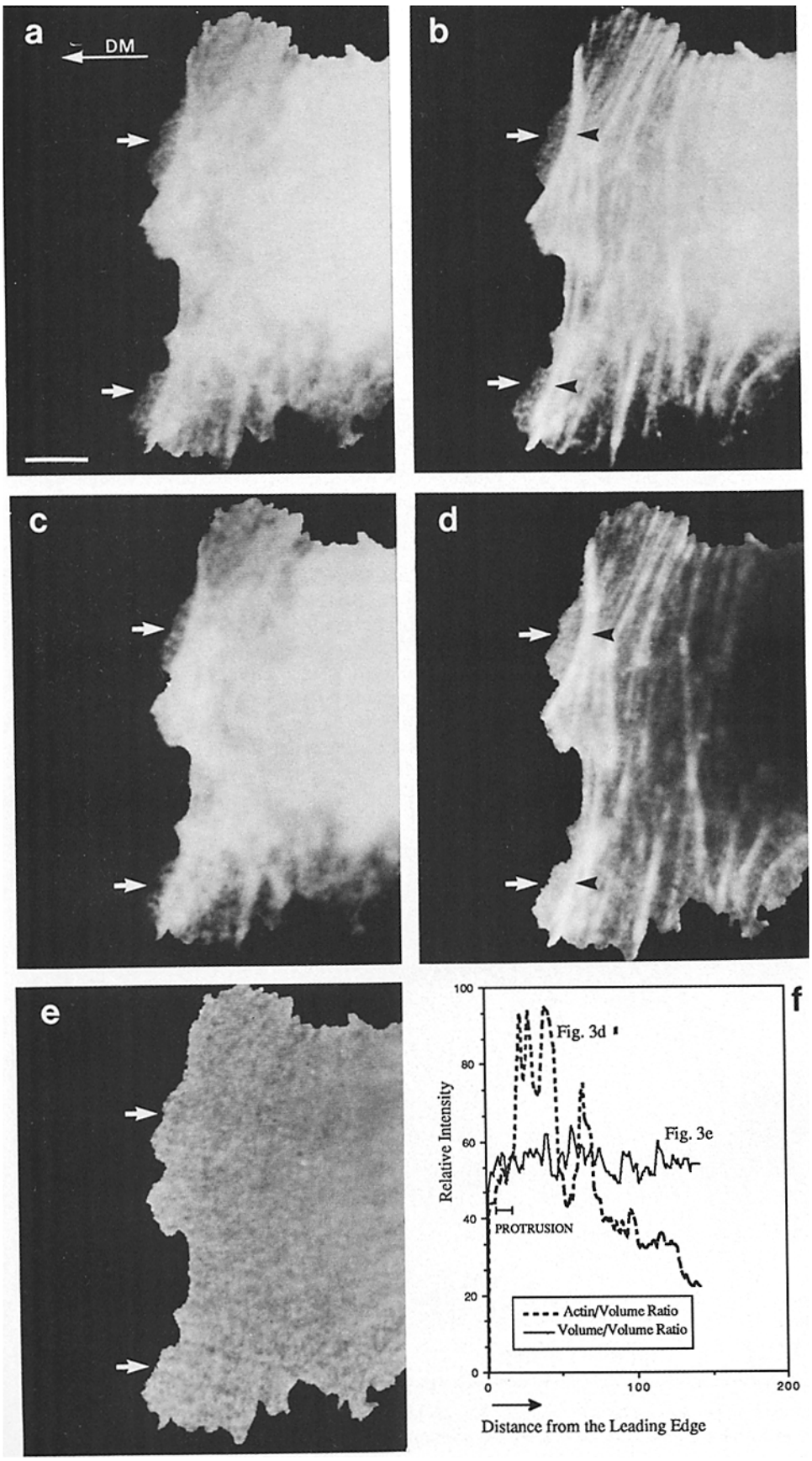

Figure 3. Images of 3T3 fibroblasts injected with AR-actin and the volume indicator FL-dextran-5K. Images were acquired 2.5 h after wounding. (*a*) First volume indicator image showed the location of two initial protrusions on the same cell (*white arrows*). (*b*) Actin image displayed diffuse actin fluorescence throughout both initial protrusions (*white arrows*) and transverse fibers at the base of each protrusion (*black arrowheads*). A two-color composite of *a* and *b* is shown in Fig. 4 *a*. (*c*) Second volume image taken after the actin image verified the continued presence of the initial protrusions. (*d*) Ratio image of actin/volume-1 indicated an elevated, but relatively uniform intensity within the initial protrusion reflecting an elevated and uniform actin distribution within this region (*white arrows*). A relative concentration of actin in the form of transverse fibers was noted at the base of each initial protrusion (*black arrowheads*). (*e*) Ratio image of volume-2/volume-1 indicated no motion artefacts and validated the use of ratio imaging to determine relative concentration. (*f*) Scan line data through actin/volume-1 ratio (*d*) at the upper protrusion, and through volume-2/volume-1 ratio (*e*) at the same location. *DM*, direction of migration. Bar, 7 μm.

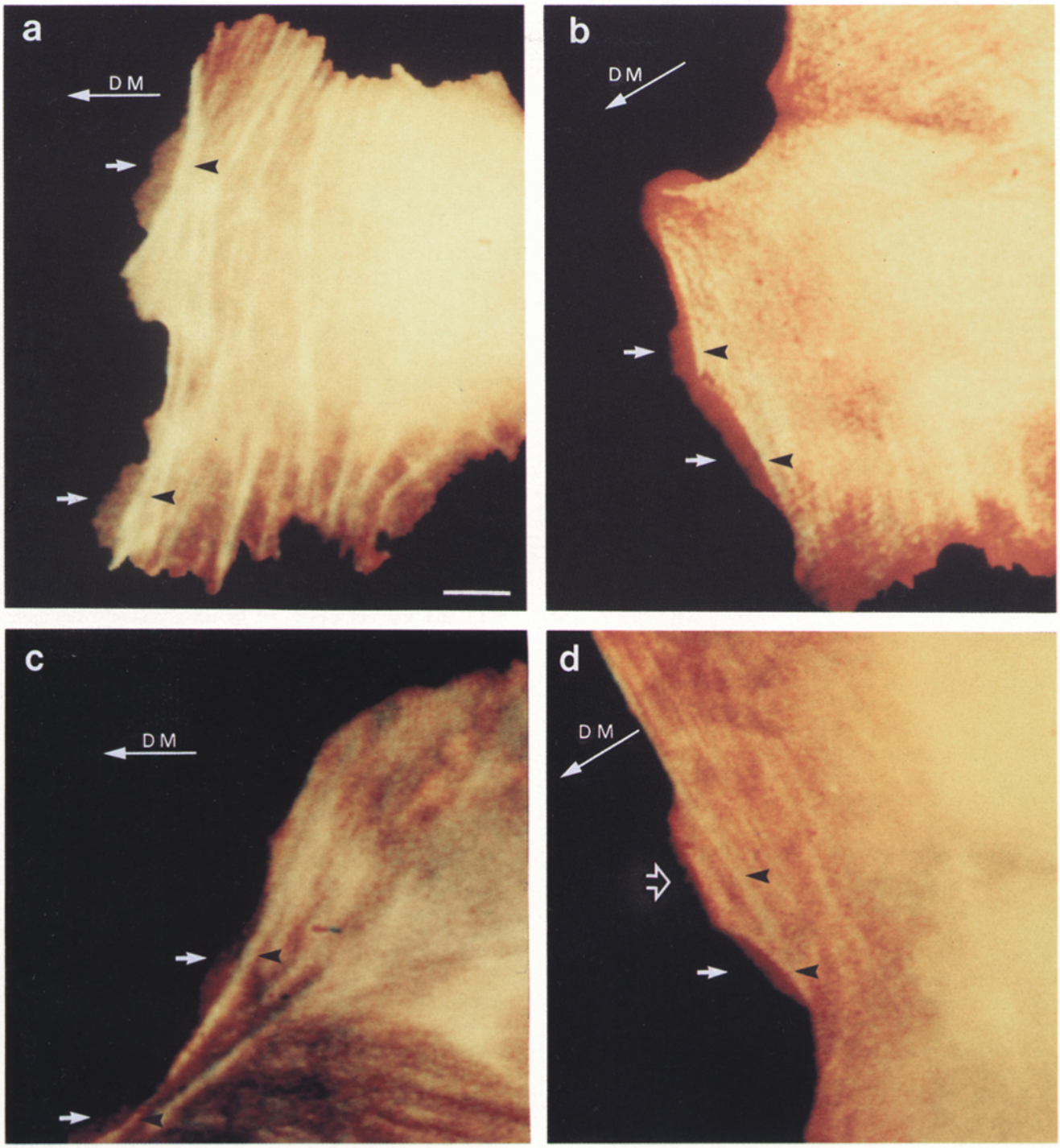

Figure 4. Simultaneous display of two computer-generated color images demonstrated the position and distribution of actin and/or myosin in protrusions at the leading edge of SW3T3 fibroblasts. A yellow color resulted when the red image and the green image contained regions of similar intensity. (*a*) Actin image (*green*) and the first volume image (*red*; see Fig. 3, *a* and *b*) showed the presence of actin in the initial protrusions (*white arrows*) and the transverse fibers near the base of the protrusions (*black arrowheads*). (*b*) Myosin image (*green*) and the first volume image (*red*; see Fig. 5, *a* and *b*) indicated the absence of myosin in the initial protrusions (*white arrows*) and the presence of myosin in transverse fibers located at the base of initial protrusions (*black arrowheads*). (*c*) Actin image (*red*) and the myosin image (*green*; see Fig. 7, *a* and *b*) showed the presence of actin, the absence of myosin in the initial protrusions (*white arrows*), and the colocalization of actin and myosin along transverse fibers near the base of the initial protrusions (*black arrowheads*). (*d*) Myosin image (*green*) and the volume image (*red*; see Fig. 7, *c* and *d*) demonstrated the presence and distribution of myosin in an established protrusion (*open arrow*). An initial protrusion (*white arrow*) formed adjacent to the established protrusion and transverse fibers were observed near the base of both protrusions (*black arrowheads*). *DM*, direction of migration. Bar, 6 μm.

(Fig. 3 *d*) at the level of the upper arrow including the initial protrusions demonstrates that actin is slightly concentrated in the initial protrusion and actin is less concentrated in more posterior regions of the cell devoid of transverse fibers (see Fig. 3, *d* and *f*).

The uniform gray scale values of the initial protrusions in the actin/volume ratio image (Fig. 3 *d*), as well as the uniform fluorescence pattern in the protrusions observed in the raw volume and actin images (Fig. 3, *a–c*, *white arrows*) indicated a relatively uniform distribution of actin throughout protrusions. Initial protrusions did not exhibit detectable actin fibers or microspikes large enough to be detected at the present level of resolution. However, these data demonstrated that actin was concentrated in the protrusion relative to the volume control.

The actin/volume ratio image also indicated an increased relative concentration of actin at the base of most initial protrusions (Fig. 3 *d*, *black arrowheads*) in the form of transverse fibers, possibly similar to the arcs described by Heath et al. (1983) and Sorrano and Bell (1982). Numerous transverse fibers containing actin were aligned perpendicular to the direction of migration from the base of the protrusion to an area in front of the nucleus.

The ratio of the two volume images (Fig. 3 *e*) displayed a relatively uniform value, indicating no major change in the extension or retraction of protrusions during the sequence of image acquisition. In some experiments, the second volume image indicated the retraction of the protrusion. Since it was not clear if retraction had commenced before, during, or after the actin image, sequences were discarded if they did not demonstrate a relatively stable protrusion in the second volume image. In addition, the relatively flat volume/volume ratio (Fig. 3, *e* and *f*) validates the use of ratio measurements to define local, relative concentration.

Distribution of Myosin in Initial Protrusions

Initial protrusions were observed along the leading edge of a cell that was migrating into the wound (Fig. 5 *a*, *white arrows*). Myosin was absent or present in low levels near the base of the protrusions (Fig. 5 *b*, *white arrows*). When low levels of myosin were observed, the fluorescence pattern was diffuse, or punctate with no well-defined, detectable structures. However, numerous transverse fibers behind the initial protrusion displayed a punctate, periodic myosin fluorescence pattern (Fig. 5 *b*, *black arrowheads*). Diffuse myosin fluorescence was observed throughout most of the cell, particularly in the perinuclear region (Fig. 5 *b*). A two-color composite image of Fig. 5, *a* and *b* is shown in Fig. 4 *b*.

The myosin ratio image demonstrated the absence or extremely low levels of myosin in the regions of the initial protrusions (Fig. 5, *d* and *f*, *white arrows*). Therefore, myosin was not detected when the cell membrane extended forward during initial protrusion, however, low levels of diffuse myosin were occasionally observed at the base of the protrusion on the anterior side of the transverse fibers. This result is in contrast to the actin ratio image which indicated a relative increase in actin concentration within the initial protrusion (compare Fig. 3, *d* and *f* with Fig. 5, *d* and *f*, *white arrows*). High relative concentrations of myosin were observed near the base of the protrusion often in the form of concave transverse fibers (Fig. 5 *d*, *black arrowheads*).

The volume ratio (Fig. 5 *e*) indicated once again that significant movements did not occur during the period of image acqusition. Therefore, the temporal resolution of these experiments was adequate to analyze the organization of myosin relative to the volume control. Slight movement of a ruffle in an anterior region of the cell occurred during image acquisition and was detected as a change in the pathlength in the volume images, but this region was behind the initial protrusion and was not analyzed (Fig. 5 *e*, *small black arrowhead*).

Distribution of Actin and Myosin in the Same Initial Protrusion

We have shown that actin is slightly concentrated, whereas myosin is relatively excluded from initial protrusions when compared to the volume control. A direct demonstration of the relative distribution of actin and myosin was accomplished through the incorporation of both actin and myosin analogues in the same cell. The above studies demonstrated that diffuse actin was always found throughout initial protrusions. Therefore, in these studies the actin image was used to identify the location of initial protrusions (Fig. 6 *a*, *white arrows*).

Cells containing both actin and myosin analogues demonstrated the presence of actin (Fig. 6 *a*), the absence of detectable levels of myosin (Fig. 6 *b*) within the same initial protrusion, and the colocalization of actin and myosin along concave transverse fibers near the base of initial protrusions. These anterior, concave, transverse fibers always became rectilinear with time. A two-color composite of Fig. 6, *a* and *b* is shown in Fig. 4 *c*.

Distribution of Myosin in Established Protrusions

Multiple episodes of extension and retraction were detected in the volume fluorescence images as an increase in pathlength at the leading edge (Fig. 7 *a*, *white arrows*). During the retraction of the protrusion, the regions of increased volume often moved centripetally (Fig. 7 *a*, *black arrowheads*). Diffuse myosin fluorescence was present at the leading edge and in all areas corresponding to increased pathlength during ruffling activity (Fig. 7 *b*, *white arrows and black arrowheads*). The retraction of a large, relatively slow moving protrusion (Fig. 7 *c*, *white arrow*) exhibited regions containing myosin at the leading edge that corresponded to regions of increased pathlength (Fig. 7, *c* and *d*, *white arrowheads*). Two transverse fibers containing myosin were detected at the base of the protrusion (Fig. 7 *d*, *black arrowheads*).

Multiple protrusions can occur simultaneously at adjacent sites along the leading edge. They can merge into a single protrusion or one may retract yielding predominant forward directional movement to the other protrusion. Although protrusions can coexist at adjacent sites, they frequently are initiated simultaneously. Protrusions at various temporal stages were often observed along the same leading edge. The distribution of myosin within the protrusions reflected these temporal stages. An established protrusion engaged in ruffling activity is shown in Fig. 7 *e* (*white arrow*). Myosin was observed throughout most of the established protrusion and was also localized in the retracting ruffle (Fig. 7, *e* and *f*, *black arrowheads*). An initial protrusion (Fig. 7 *e*, *open arrow*) formed next to the established protrusion and had no detectable myosin fluorescence (Fig. 7 *f*, *open arrow*). Transverse fibers containing myosin were located at the base of both the

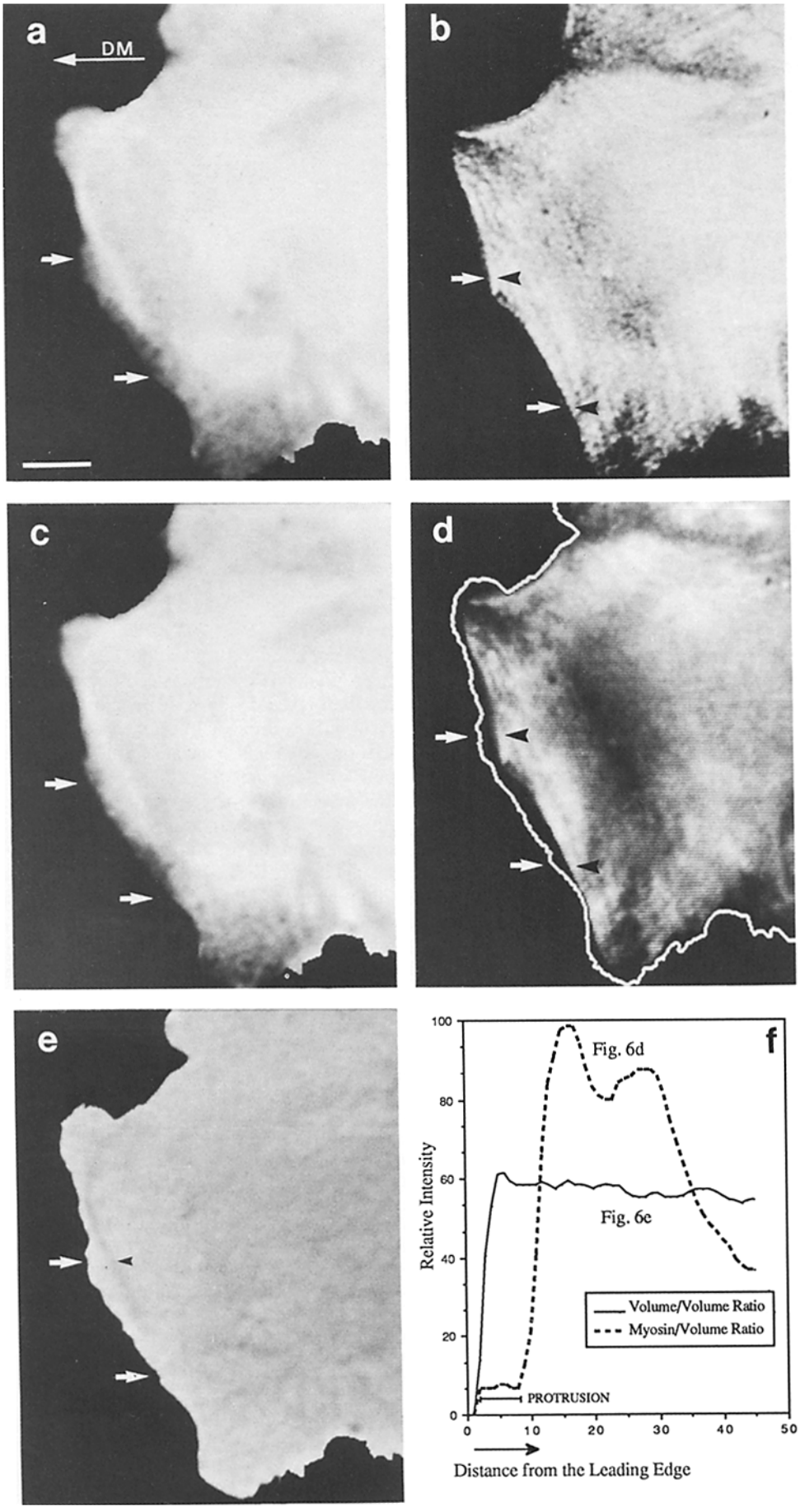

Figure 5. Images of 3T3 fibroblasts injected with AR-myosin and the volume indicator FL-dextran-5K. Images were acquired 2.5 h after wounding. (*a*) First volume image identified the location of the initial protrusions (*white arrows*). (*b*) Myosin image showed the absence of myosin in the initial protrusions (*white arrows*) and the presence of myosin in the transverse fibers located near the base of the initial protrusions (*black arrowheads*). A display of *a* and *b* in a two-color composite is provided in Fig. 4 *b*. (*c*) Second volume image indicated that the initial protrusions had not moved significantly during image acquisition. (*d*) Ratio image of myosin/volume-1. The low ratio in the region of the initial protrusion reflected the absence or low levels of myosin in these regions (*white arrows*; an outline delineated the peripheral cell edge). At the base of the initial protrusions, high relative concentrations of myosin were observed in the form of concave transverse fibers (*black arrowheads*). (*e*) Ratio image of volume-2/volume-1 displayed no major volume change (extension or retraction) of the initial protrusions (*white arrows*), however a region in the extending lamellum showed a change in pathlength and was detected on the ratio image (*small black arrowhead*). (*f*) Scan line data through the myosin/volume-1 ratio (Fig. 5 *d*) at the center of the protrusion, and through the volume-2/volume-1 ratio (Fig. 5 *e*) at the same location. *DM*, direction of migration. Bar, 7 μm.

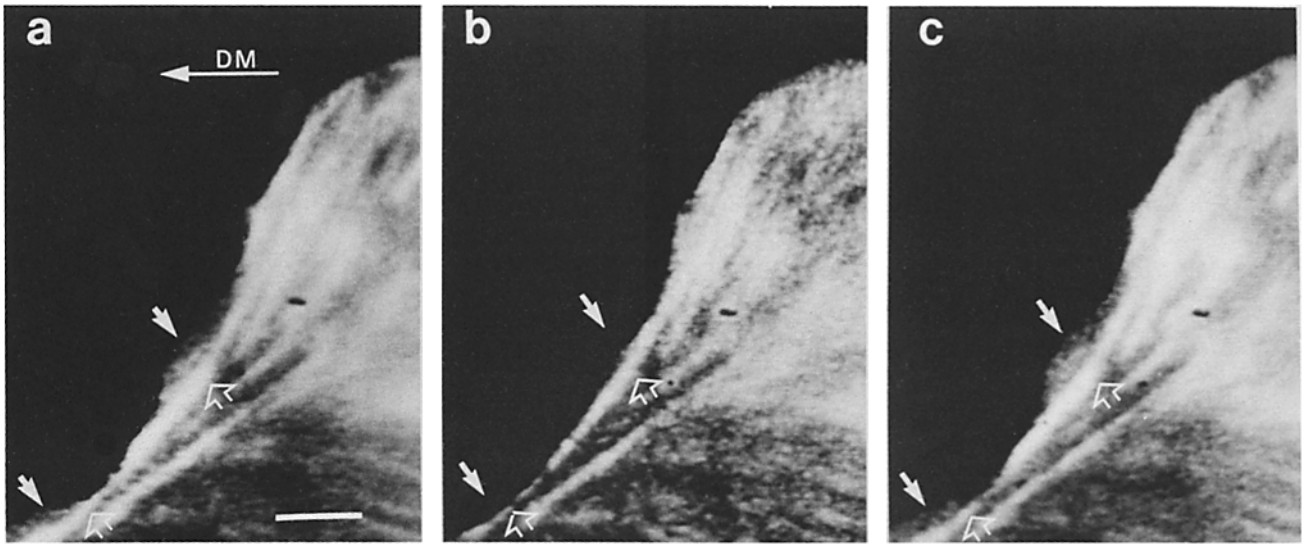

Figure 6. 3T3 fibroblasts labeled with both AF-actin and AR-myosin. Images were acquired 4 h after wounding. (*a*) First actin image identified the initial protrusions (*white solid arrows*) and transverse fibers near the base of the initial protrusions (*open arrows*). (*b*) Myosin image displayed the absence of myosin in the region of the initial protrusions (*white solid arrows*) and the transverse fibers near the base of the protrusions (*open arrows*). A two-color composite of Fig. 6, *a* and *b*, is displayed in Fig. 4 *c*. (*c*) Second actin image verified the continued presence of the initial protrusions (*white arrows*). *DM*, direction of migration. Bar, 7 μm.

initial and established protrusions (Fig. 7 *f*, *black arrows*). The color composite in Fig. 4 *d* indicates the distribution of myosin in an established protrusion.

Protrusions can remain stationary after initial extension or after multiple episodes of retraction/extension, which might be important in establishing directional movement along the substrate. Fig. 7 *g* (*white arrow*) shows the volume fluorescence image of a relatively stable, stationary established protrusion. Myosin-containing structures within stationary established protrusions were often observed in a "/\"-shaped configuration, with the tip pointing towards the direction of migration (Fig. 7 *h*; see also Fig. 1 *c*, *small arrow*, and Fig. 8 *d*, *arrowheads*).

Dynamics of Myosin Penetration into Stationary Established Protrusions

The first volume image demonstrated an initial protrusion that contained no detectable myosin (Fig. 8, *a* and *b*). After 1 min, myosin was detected in diffuse and punctate forms in the region of the protrusion (Fig. 8 *c*). A subsequent image of the same protrusion taken 1 min later demonstrated the presence of myosin with a stronger fluorescence signal, in a more organized, periodic, and punctate form (Fig. 8 *d*). When the second volume fluorescence image (Fig. 8 *e*) was overlayed onto the first volume image (overlay not shown), the position of the protrusion had not appreciably changed during the image acquisition series. Therefore, myosin appears to penetrate into protrusions after their formation. To avoid possible illumination trauma to the cell, fluorescein volume images were not acquired at each time point. Observations of the volume control marker at 20-s intervals indicated that the protrusion did not appear to be engaged in significant retraction or ruffling activity.

Myosin Fluorescence Photobleaching Recovery

The fluorescence photobleaching recovery technique pro-

Figure 7. The distribution of myosin in established protrusions. 3T3 cells were microinjected with AR-myosin and the volume indicator FL-dextran-5K. Images were acquired 3 h after wounding. Cell 1: (*a*) The volume indicator image displayed regions of ruffling activity along the leading edge (*white arrows*). Areas of increased pathlength, resulting from retraction of the protrusion, moved back towards the nucleus (*black arrowheads*). (*b*) The myosin image exhibited diffuse myosin fluorescence at the leading edge and in regions corresponding to the increased pathlength (*white arrows and black arrowheads*). Cell 2: (*c*) The volume fluorescence image indicated a large protrusion (*white arrow*) that was retracting, and areas of increased pathlength were observed at the leading peripheral edge of the protrusion (*white arrowheads*). (*d*) The myosin image demonstrated areas of increased myosin fluorescence along the leading edge of the protrusion corresponding to regions of increased pathlength (*small white arrowheads*). Two groups of transverse fibers were observed at the base of the protrusion (*black arrowheads*). Cell 3: (*e*) The volume image revealed an established protrusion engaged in ruffling activity (*white arrow*) and an initial protrusion (*open arrow*) forming at an adjacent site. (*f*) Diffuse myosin was distributed throughout the established protrusion (*white arrow*) and the retracting ruffle (*black arrowhead*). No myosin was detected in the initial protrusion (*open arrow*). Transverse fibers were observed near the base of both the established and initial protrusions (*black arrows*). See Fig. 4 *d* for color composite of volume and myosin images. Cell 4: (*g*) The volume image displayed a stationary established protrusion (*white arrow*) with new protrusive activity occurring at the edges of the stationary protrusion. (*h*) Diffuse myosin fluorescence was detected in the protrusion and structures were observed along the peripheral edge of the protrusion in a "/\"-shaped configuration (*white arrowheads*). *DM*, direction of migration. Bars, 7 μm.

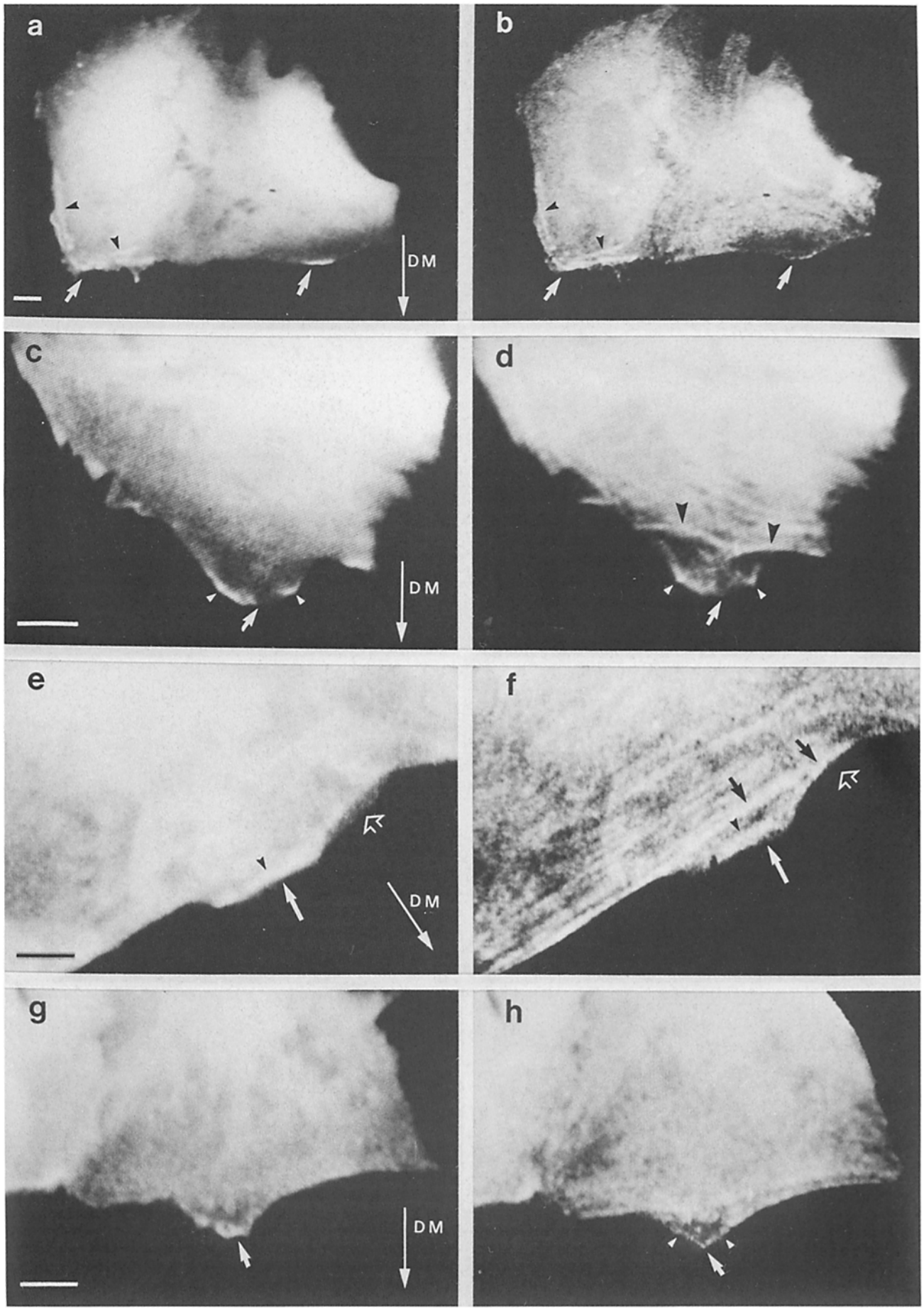
a
DM
b
c
DM
d
e
DM
f
g
DM
h

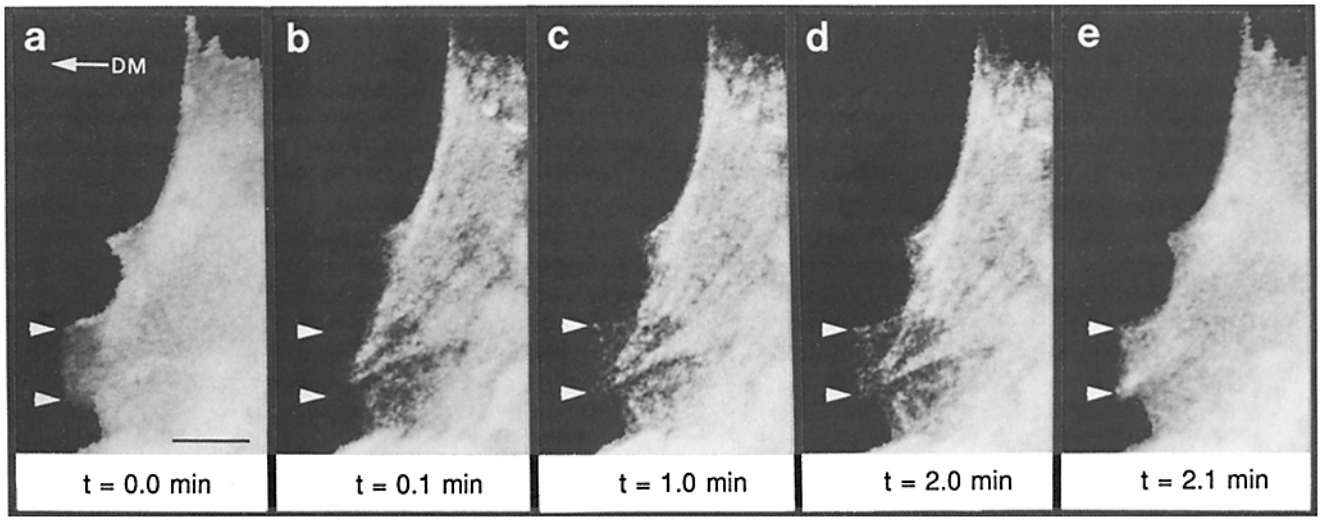

Figure 8. The dynamics of myosin penetration into a protrusion. Polarized SW3T3 fibroblasts were microinjected with AR-myosin and FL-dextran-5K and sequential images were acquired 2.5 h after wounding. (*a*) Volume fluorescence image of a cell containing an initial protrusion (*upper and lower edges marked by arrowheads*). (*b*) Myosin image demonstrated the absence of myosin in the initial protrusion. (*c*) Myosin was present as diffuse fluorescence and points of fluorescence after 1 min. (*d*) Myosin was noted in more organized periodic structures 1 min later. (*e*) Volume fluorescence image, taken immediately after the last myosin image, indicated that the protrusion did not change significantly over the 2-min examination period. *DM*, direction of migration. *t*, time. Bar, 7 μm.

vided data on the translational mobility and percent mobile fraction of the fluorescent analogue of myosin. Determining the mobility of myosin at the leading edge of the cell would indicate the fraction of "soluble" myosin readily available for penetration into the protrusion. The myosin was 100% immobile in the tens of seconds time frame in regions near the leading edge (Fig. 9). In contrast, perinuclear regions contained only a 21% immobile fraction and the translational mobility of this fraction was 4.1×10^{-9} cm²/s (37°C). The relative immobility of myosin in the time scale of the measurements indicates that myosin is much less mobile at the leading edge of cells compared to the perinuclear region. This characteristic was observed in the analyses of 13 separate cells of which Fig. 9 is one example.

Discussion

Myosin Analogue

We have prepared fluorescent analogues of smooth muscle myosin as a probe of the distribution and assembly of standard myosin (myosin II) in cells. An analogue of smooth muscle myosin was chosen since smooth muscle myosin is now reasonably well-characterized and can be made soluble at physiological ionic strength. The analogue can be prepared in large amounts, and the coassembly of classical myosin from different sources is dominated by the species at the highest concentration (Pollard, 1975, 1981). The present level of characterization indicates that the myosin analogue exhibits properties similar to native myosin.

The smooth muscle myosin analogues were incorporated into stress fibers, and exhibited the semi-sarcomeric distribution expected from myosin, based on immunofluorescence studies (Mittal et al., 1987). Since the myosin analogue was delivered to cells at 10% of the endogenous myosin concentration, the endogenous myosin should dominate the assembly properties. We will extend the present studies in the future by comparing the distribution and mobilities of distinct types of myosin in the same cells.

Actin and Myosin in Protrusions

Fluorescent analogue cytochemistry can be used to identify the temporal and spatial changes in the subcellular distribution of specific proteins (see Taylor et al., 1986). Multiple parameter analysis provides a method to correlate the distributions of several cellular components in one cell, and ratio imaging quantifies the relative concentrations of labeled molecules by normalizing for differences in pathlength and accessible volume. Fluorescence photobleaching recovery assesses the mobility of labeled molecules in different locations of the cell. These techniques were used to address the temporal and spatial changes in the distribution and mobility of actin and myosin in living, polarized fibroblasts.

Although an elevated concentration of actin was found in initial protrusions, no well-defined structures within initial protrusions were observed by fluorescence or by VEC microscopy. VEC microscopy demonstrated the presence (Fig. 2, *b* and *c*) and movement of actin-containing fibers and microspikes (Fisher et al., 1988) that become visible in established protrusions. Electron microscopy (Small, 1981) demonstrated the intricate network of actin filaments and microspikes in the leading edge of cultured fibroblasts.

Ratio imaging indicated that myosin was either absent, or present in extremely low levels in initial protrusions. However, increased concentrations of myosin in the form of concave transverse fibers were detected near the base of initial protrusions. Actin levels were elevated in initial protrusions compared to other regions of the cell devoid of actin-containing fibers. When the same cells were labeled with both myosin and actin, the initial protrusions showed the presence of actin throughout the protrusion, and the relative absence of

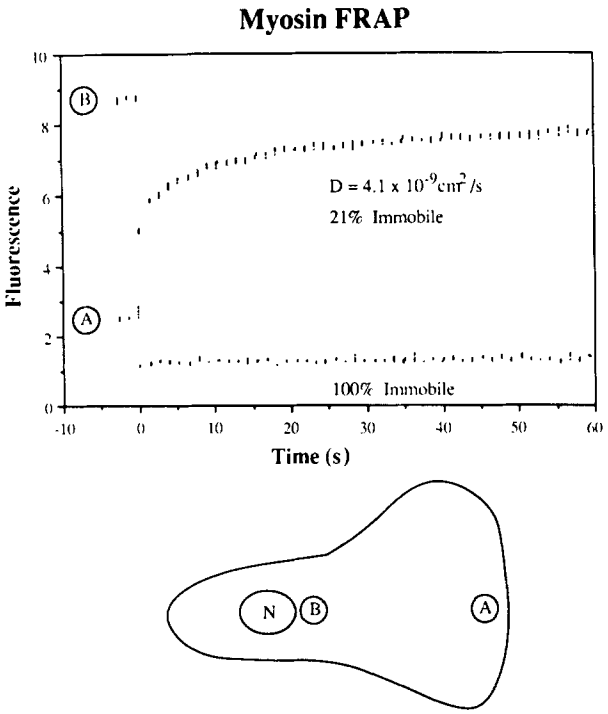

Figure 9. Myosin fluorescence after photobleaching. 3 h after wounding, AF-myosin-labeled 3T3 cells were photobleached with a 6-μm radius laser spot in regions near the leading edge (*A*) and in front of the nucleus (*B*). The myosin near the leading edge was 100% immobile during the time (60 s) of measurement. In contrast, the myosin in the anterior perinuclear region exhibited a 21% immobile fraction and the translational mobility of this fraction was 4.1×10^{-9} cm²/s (37°C).

myosin in the same region (Fig. 6). The actin and myosin images showed transverse fibers at the base of the initial protrusions, and the two-color composite (Fig. 4 *c*) demonstrated the colocalization of actin and myosin along these fibers at the base of initial protrusions. Therefore, initial protrusions involve a local, relative increase in the actin concentration and do not appear to require detectable myosin II-containing structures within the protrusion.

Penetration of Myosin in Established Protrusions

Although myosin was absent from initial protrusions, the myosin analogue was detected in established protrusions as both diffuse and punctate fluorescence (Figs. 7 and 8). Diffuse myosin was observed in ruffles at the leading edge of migrating cells and myosin was detected as a meshwork or in discreet structures in the leading edge of migrating cells without protrusions and in older, established protrusions that remained attached to the substrate. The delayed penetration of myosin into established protrusions generated several questions including: (*a*) how is myosin restricted from entering initial protrusions even though it is present throughout the adjacent extending lamellum?; (*b*) what are the possible mechanisms for the eventual penetration of myosin into established protrusions?; and (*c*) could transverse fibers containing actin and myosin at the base of the protrusion play a role in the formation of protrusions?

Cytoplasmic compartmentalization of size fractionated ficolls in spreading fibroblasts has been studied by showing the penetration of 3.5 nm (hydrodynamic radius) ficoll molecules and the exclusion of 25.0 nm ficolls from the peripheral edges of fibroblasts (Luby-Phelps and Taylor, 1988). The size of monomeric actin is ~4.0 × 4.0 × 6.5 nm (Milligan and Flicker, 1987). The labeled actin in the cell could (*a*) bind to profilin-like proteins (but not profilin; Malm, 1984) and maintain its monomeric configuration, (*b*) form short filaments stimulated by barbed-end actin-binding proteins (gelsolin), and/or (*c*) exchange into existing actin cytoskeletal structures (Amato and Taylor, 1986). The extending lamellum contains a large mobile fraction of actin even in regions with fibers (Amato and Taylor, 1986; Wang, 1985). This mobile fraction could diffuse into the initial protrusions as they form (Fig. 3). The diffusion of actin could occur due to the small size of the actin species. Actin oligomers might also be capable of diffusing through the cytoplasm into the initial protrusion.

Considering the molecular size and configuration of myosin, it may be excluded sterically from initial protrusions by the cytoplasmic network in this thin region. Smooth muscle myosin can exist in various configurations, including the antiparallel dimeric myosin filament, the 10S folded monomeric myosin, and the extended 6S monomer under physiological conditions (Trybus and Lowey, 1984, 1987*a*, *b*). The head region of the extended 6S monomer is ~13 × 18 nm with a tail 2 nm wide and 150 nm long. The most compact folded monomer, with the tail folded parallel to the head forming a hairpin structure (Onishi and Wakabayashi, 1982), would be at least 18 nm wide and ~50–60 nm long (Flicker et al., 1983). Therefore, the size of the most compact myosin monomer is considerably larger than an actin monomer. Since labeled ficoll molecules with a hydrodynamic radius of 25.0 nm were unable to penetrate into thin regions of the cell periphery, labeled myosin might also encounter restricted diffusion through the cytoplasm into the initial protrusions. The delay in the appearance of myosin in established protrusions might reflect the restricted mobility of such a large protein through a restrictive cytoplasmic network within the protrusion, in addition to the affinity of myosin for actin in this actin rich area.

Photobleaching data demonstrated that the myosin was relatively immobile in and around the transverse fibers at the front of the leading lamellum of cells. This finding suggests that the cytoplasmic network in this region restricts the myosin from penetrating into this area and/or that myosin is bound to structures and is not readily available for diffusion into the protrusion. Myosin might require an active transport mechanism that mobilizes myosin into the established protrusion by specific molecular interactions, possibly with actin already present in the protrusion.

Myosin might also penetrate into the protrusions by "crawling" along the newly formed actin filaments or microspikes that extend into the established protrusion. Actin assembly probably occurs at the barbed end of actin filaments which are oriented towards the leading edge (Small et al., 1978). The delayed appearance of myosin in protrusions might reflect the time needed for myosin to move towards the barbed, distal end of the actin filaments. The distribution of myosin in slow forming initial protrusions often shows diffuse myosin fluorescence located in the rear of the protru-

sion. This finding is consistent with the proposal of myosin moving along the network of actin filaments out towards the distal region of the protrusion. However, it has recently been demonstrated that a continuous retrograde or centripetal transport of actin occurs in the leading lamellipodia (Fisher et al., 1988). Therefore, the centrifugal penetration of myosin into lamellipodia is occurring against the centripetal transport of actin.

Implications on the Mechanism of Forming Protrusions

Theories on the forces responsible for protrusions in amoeboid cells include: (*a*) turgor pressure in the lamellipodia as a result of an increase in osmotic pressure causing an influx of water (Oster, 1984); (*b*) positive hydrostatic pressure generated by the contraction of a more posterior region (Chen, 1981; Taylor et al., 1980*a*,*b*; Mast, 1926; Taylor and Condeelis, 1979); (*c*) interaction of actin and myosin within the protrusion producing frontal contractile forces that drive the leading cytoplasmic membrane forward (Huxley, 1973; Allen, 1961); (*d*) insertion of membrane at the leading edge by membrane recycling through polarized exocytosis/endocytosis processes (Singer and Kupfer, 1986; Abercrombie et al., 1970*a*,*b*); and (*e*), rapid actin polymerization which structurally drives the forward extension of the protrusion (Tilney and Kallenbach, 1979; Inoue and Tilney, 1982). In addition, it is also possible that another form of myosin interacts with actin to generate force (Collins and Borysenko, 1984; Conzelman and Mooseker, 1987; Albanesi et al., 1985).

The present results appear consistent with the possible role of turgor pressure, hydrostatic pressure, and actin assembly in the formation of protrusions at the leading edge of lamellipodia. The results are inconsistent with a direct interaction of actin and standard myosin (myosin II) in the leading edge since myosin does not enter the protrusion until it has become "established." The absence of membrane vesicles directed forward into initial protrusions also leaves some doubt about the exact location of any membrane insertion at the leading edge of migrating cells (Fisher et al., 1988).

The colocalization of actin and myosin in transverse fibers at the base of protrusions suggests a possible site for a contractile force that might participate in the formation and/or maintenance of protrusions. Any force generated by the transverse fibers could also be directly involved in generating local pressure at the site of contraction and possibly reorganization of the cytoplasm in the lamellipodia. The transverse fibers might be analogous to the plasma gel sheets that form at the tips of advancing pseudopods in amoebae which are believed to both decrease the gel structure at the leading edge of pseudopods and control the direction of migration (Taylor et al., 1980*a*,*b*; Taylor and Fechheimer, 1982). The concave configuration of most of the transverse fibers at the base of initial protrusions might result from force generation and the asymmetric shortening of the fibers during force generating contractions. Local measurements of force will be required to answer this issue.

The increase in the relative concentration of actin in initial protrusions (Fig. 3) is consistent with an assembly of actin that could concentrate actin in local domains. The slow rate of extension of lamellipodial protrusions (~2–5 μm/min), (Fisher et al., 1988) makes it possible that actin assembly at the barbed ends of actin associated with the membrane, could play a major role in forming and/or maintaining the protrusions. Alternatively, actin assembly could occur in concert with increased turgor pressure and/or positive hydrostatic pressure (Oster and Perelson, 1987), and/or actin interaction with a second class of myosin (myosin I) (Collins and Borysenko, 1984; Conzelman and Mooseker, 1987; Albanesi et al., 1985).

Our predictions suggest that some chemical messenger(s), (i.e., pH, pCa, components of the lipid metabolism pathway, or phosphorylation) act locally at the site of a "desired" new protrusion to initiate the sequence of events required to form the protrusion. We have not yet identified any spatial variation in pH at the sites of protrusions (Bright, G. R. and D. L. Taylor, unpublished observations). Transient elevations of calcium at the sites of new protrusions have been identified in amoebae (Taylor et al., 1980*b*) and the mechanisms might be analogous. Future multiple parameter studies will integrate measurements of ionic properties with the dynamics of selected cytoskeletal proteins (Taylor et al., 1986; DeBiasio et al., 1987).

The authors express their appreciation to Charlotte Bartosh, Ray Griffith, Judy Montibeller, Hung Nguyen, and Chris Thompson for expert technical assistance. We thank S. Lowey and K. Trybus for their communications involving the preparation of myosin minifilaments, and Michel Nederlof and Kevin Ryan for their assistance in image processing.

This research was supported by National Institutes of Health (NIH) Program Project GM34639, NIH AM32461, Council for Tobacco Research USA, Inc. 2044, National Science Foundation and NIH equipment grants BBS-8609687, 1S10 RR03377, and a National Science Foundation facilities center grant BBS-8714181.

Received for publication 24 March 1988, and in revised form 6 September 1988.

References

Abercrombie, M., J. E. Heaysman, and S. M. Pegrum. 1970*a*. The locomotion of fibroblasts in culture. I. Movements of the leading edge. *Exp. Cell Res.* 59:393–398.

Abercrombie, M., J. E. Heaysman, and S. M. Pegrum. 1970*b*. The locomotion of fibroblasts in culture. II. Ruffling. *Exp. Cell Res.* 60:437–444.

Albanesi, J. P., H. Fujisaki, and E. D. Korn. 1985. A kinetic model for the molecular basis of the contractile activity of *Acanthamoeba* myosins IA and IB. *J. Biol. Chem.* 260:11174–11179.

Allen, R. D. 1961. Amoeboid movement. *In* The Cell. J. Brachet and A. E. Mirsky, editors. Academic Press, Inc., New York. 135–216.

Amato, P. A., and D. L. Taylor. 1986. Probing the mechanism of incorporation of fluorescently labeled actin into stress fibers. *J. Cell Biol.* 102:1074–1084.

Amato, P. A., E. R. Unanue, and D. L. Taylor. 1983. Distribution of actin in spreading macrophages: a comparative study on living and fixed cells. *J. Cell Biol.* 96:750–761.

Bradford, M. M. 1976. A Rapid and sensitive method for the quantitation of microgram quantities of protein utilizing the principle of protein-dye binding. *Anal. Biochem.* 72:248–254.

Bright, G. R., G. W. Fisher, J. Rogowska, and D. L. Taylor. 1987. Fluorescence ratio imaging microscopy. Temporal and spatial measurements of cytoplasmic pH. *J. Cell Biol.* 104:1019–1033.

Castleman, K. R. 1979. Digital Image Processing. Prentice-Hall Inc., Englewood Cliffs, NJ. 226–249.

Chen, W.-T. 1981. Mechanism of the retraction of the trailing edge during fibroblast movement. *J. Cell Biol.* 90:187–200.

Collins, J. H., and C. W. Borysenko. 1984. The 110,000-dalton actin- and calmodulin-binding protein from intestinal brush border is a myosin-like ATPase. *J. Biol. Chem.* 259:14128–14135.

Conzelman, K. A., and M. S. Mooseker. 1987. The 110-kD protein-calmodulin complex of the intestinal microvillus is an actin-activated MgATPase. *J. Cell Biol.* 105:313–324.

David-Pfeuty, T. 1985. The coordinate organization of vinculin and of actin filaments during the early stages of fibroblast spreading on a substratum. *Eur. J. Cell Biol.* 36:195–200.

DeBiasio, R. L., G. R. Bright, L. A. Ernst, A. S. Waggoner, and D. L. Taylor. 1987. Five-parameter fluorescence imaging: wound healing of living Swiss 3T3 cells. *J. Cell Biol.* 105:1613–1622.

Fisher, G. W., P. Conrad, R. L. DeBiasio, and D. L. Taylor. 1988. Centripetal transport of cytoplasm, actin, and the cell surface in lamellipodia of fibroblasts. *Cell Motil. Cytoskeleton.* In press.

Flicker, P. F., T. Wallimann, and P. Vibert. 1983. Electron microscopy of scallop myosin: location of regulatory light chains. *J. Mol. Biol.* 169:723–741.

Geiger, B., Z. Avnur, G. Rinnerthaller, H. Hinssen, and V. J. Small. 1984. Microfilament-organizing centers in areas of cell contact: cytoskeletal interactions during cell attachment and locomotion. *J. Cell Biol.* 99 (Suppl.): 83–91.

Gotlieb, A. I., M. H. Heggeness, J. F. Ash, and S. J. Singer. 1979. Mechanochemical proteins, cell motility and cell–cell contact: the localization of mechanochemical proteins inside cultured cells at the edge of an in vitro "wound." *J. Cell Physiol.* 100:563–578.

Heath, J. P. 1983. Behavior and structure of the leading lamella in moving fibroblasts. I. Occurrence and centripetal movement of arc-shaped microfilament bundles beneath the dorsal cell surface. *J. Cell Biol.* 60:331–354.

Heggeness, M. H., K. Wang, and S. J. Singer. 1977. Intracellular distributions of mechanochemical proteins in cultured fibroblasts. *Proc. Natl. Acad. Sci. USA.* 74:3883–3887.

Herman, I. M., N. J. Crisona, and T. D. Pollard. 1981. Relation between cell activity and the distribution of cytoplasmic actin and myosin. *J. Cell Biol.* 90:84–91.

Huxley, H. E. 1973. Muscular contraction and cell motility. *Nature (Lond.).* 243:445–449.

Inoue, S., and L. G. Tilney. 1982. The acrosomal reaction of the Thyone sperm. I. Changes in the sperm head visualized by high resolution video microscopy. *J. Cell Biol.* 93:812–819.

Kolega, J. 1985. Effects of mechanical tension on protrusive activity and microfilament and intermediate filament organization in an epidermal epithelium moving in culture. *J. Cell Biol.* 102:1400–1411.

Kreis, T., B.Geiger, and J. Schlessinger. 1982. Mobility of microinjected rhodamine actin within living chicken gizzard cells determined by fluorescence photobleaching recovery. *Cell.* 29:835–845.

Laemmli, U. 1970. Cleavage of structural proteins during the assembly of the head of bacteriophage T4. *Nature (Lond.).* 227:680–685.

Letourneau, P. C. 1985. Axonal growth and guidance. *In* Molecular Bases of Neural Development. Edelman, Gal, and Cowan, editors. Neurosciences Research Foundation. 86–101.

Luby-Phelps, K., D. L. Taylor, and F. Lanni. 1986. Probing the structure of cytoplasm *J. Cell Biol.* 102:2015–2022.

Luby-Phelps, K., and D. L. Taylor. 1988. Subcellular compartmentalization by local differentiation of cytoplasmic organization. *Cell Motil. Cytoskeleton.* 10:28–37.

Luby-Phelps, K., P. E. Castle, D. L. Taylor, and F. Lanni. 1987. Hindered diffusion of inert tracer particles in the cytoplasm of living cells. *Proc. Natl. Acad. Sci. USA.* 84:4910–4913.

Luby-Phelps, K., F. Lanni, and D. L. Taylor. 1985. Behavior of a fluorescent analogue of calmodulin in living 3T3 cells. *J. Cell Biol.* 101:1245–1256.

Malm, B. 1984. Chemical modification of cys-374 of actin interferes with the formation of the profilactin complex. *FEBS (Fed. Eur. Biochem. Soc.) Letts.* 173:399–402.

Mast, S. O. 1926. Structure, movement, locomotion and stimulation in amoeba. *J. Morph. Physiol.* 41:347–425.

Milligan, R. A., and P. F. Flicker. 1987. Structural relationships of actin, myosin, and tropomyosin revealed by cryo-electron microscopy. *J. Cell Biol.* 105:29–39.

Mittal, B., J. M. Sanger, and J. W. Sanger. 1987. Visualization of myosin in living cells. *J. Cell Biol.* 105:313–324.

Mooseker, M. S., and L. G. Tilney. 1975. The organization of an actin filament-membrane complex: filament polarity and membrane attachment in the microvilli of intestinal epethelial cells. *J. Cell Biol.* 67:725–743.

Ngai, P. K., C. A. Carruthers, and M. P. Walsh. 1984. Isolation of the native form of chicken gizzard myosin light-chain kinase. *Biochem. J.* 218:863–870.

Onishi H., and T. Wakabayashi. 1982. Electron microscopic studies of myosin molecules from chiken gizzard muscle I: the formation of the intramolecular loop in the myosin tail. *J. Biochem.* 92:871–879.

Oster, G. F., and A. S. Perelson. 1987. The physics of cell motility. *J. Cell Sci.* 8(Suppl.)35–54.

Pollard, T. D. 1975. Electron microscopy of synthetic myosin filaments. *J. Cell Biol.* 67:93–104.

Pollard, T. D. 1981. Cytoplasmic contractile proteins. *J. Cell Biol.* 91(Suppl.): 156–165.

Sellers, J. R., and M. D. Pato. 1984. The binding of smooth muscle myosin light chain kinase and phosphatases to actin and myosin. *J. Biol. Chem.* 259:7740–7746.

Sellers, J. R., M. D. Pato and R. S. Adelstein. 1981. Reversible phosphorylation of smooth muscle myosin, heavy meromyosin, and platelet myosin. *J. Biol. Chem.* 256:13137–13142.

Simon, J., R. Furukawa, B. Ware, and D. Taylor. 1988. The molecular mobility of α-actinin and actin in a reconstituted model of gelation. *Cell Motil. Cytoskeleton.* 11:64–82.

Singer, S. J., and A. Kupfer. 1986. The directed migration of eukaryotic cells. *Annu. Rev. Cell Biol.* 2:337–365.

Small, J. V. 1981. Organization of actin in the leading edge of cultured cells: influence of osmium tetroxide and dehydration on the ultrastructure of actin meshworks. *J. Cell Biol.* 91:695–705.

Small, J. V., G. Isenberg, and J. E. Celis. 1978. Polarity of actin at the leading edge of cultured cells. *Nature (Lond.).* 272:638–639.

Sobieszek, A., and R. D. Bremel. 1975. Preparation and properties of vertebrate smooth-muscle myofibrils and actomyosin. *Eur. J. Biochem.* 55:49–60.

Sorrano, T., and E. Bell. 1982. Cytostructural dynamics of spreading and translocating cells. *J. Cell Biol.* 95:127–136.

Spudich, J. A., and S. Watt. 1971. The regulation of rabbit skeletal muscle contraction. *J. Biol. Chem.* 246:4866–4871.

Tait, J. F., and C. Frieden. 1982. Polymerization-induced changes in the fluorescence of actin labeled with iodoacetamidotetramethylrhodamine. *Arch. Biochem. Biophys.* 216:133–141.

Tanasugarn, L., P. McNeil, G. T. Reynolds, and D. L. Taylor. 1984. Microspectrofluorometry by digital image processing: measurement of cytoplasmic pH. *J. Cell Biol.* 98:717–724.

Taylor, D. L., and J. S. Condeelis. 1979. Cytoplasmic structure and contractility in amoeboid cells. *Int. Rev. Cytol.* 56:57–144.

Taylor, D. L., and M. Fechheimer. 1982. Cytoplasmic structure and contractility. The solation-contraction coupling hypothesis. *Philos. Trans. R. Soc. Lond.* 299:183–197.

Taylor, D. L., and Y.-L. Wang. 1978. Molecular cytochemistry incorporation of fluorescently labeled actin into living cells. *Proc. Natl. Acad. Sci. USA.* 75:857–861.

Taylor, D. L., P. A. Amato, P. L. McNeil, K. Luby-Phelps, and L. Tanasugarn. 1986. Spatial and temporal dynamics of specific molecules and ions in living cells. *In* Applications of Fluorescence in the Biomedical Sciences. D. L. Taylor, A. S. Waggoner, R. F. Murphy, F. Lanni, and R. R. Birge, editors. Alan R. Liss, Inc., New York. 347–376.

Taylor, D. L., J. Blinks, and G. T. Reynolds. 1980*a*. Contractile basis of ameboid movement. VIII. Aequorin luminescence during ameboid movement, endocytosis, and capping. *J. Cell Biol.* 86:599–603.

Taylor, D. L., J. A. Reidler Spudich, and L. Stryer. 1981. Detection of actin assembly by fluorescence energy transfer. *J. Cell Biol.* 89:362–367.

Taylor, D. L., Y.-L. Wang, and J. Heiple. 1980*b*. Contractile basis of ameboid movement. VII. Distribution of fluorescently labeled actin in living amoebae. *J. Cell Biol.* 86:590–598.

Tilney, L. G., and N. Kallenbach. 1979. Polymerization of actin filaments in the acrosomal process and how it might be determined. *J. Cell Biol.* 81:608–623.

Todaro, G., Y. Matsuya, S. Bloom, A. Robbins, and H. Green. 1967. Growth regulatory substances for animal cells in culture. *In* Growth Regulating Substances for Animal Cells in Culture. Vol. 7. V. Defendi, and M. Stoker, editors. Wistar Institute Press, Philadelphia. Wistar Institute Symposium. 87–98.

Trinkaus, J. P. 1985. Protrusive activity of the cell surface and the initiation of cell movement during morphogenesis. *Exp. Biol. Med.* 10:130–173.

Trybus, K. M., and S. Lowey. 1984. Conformational states of smooth muscle myosin. *J. Biol. Chem.* 259:8564–8571.

Trybus, K. M., and S. Lowey. 1987*a*. Assembly of smooth muscle myosin minifilaments: effects of phosphorylation and nucleotide binding. *J. Cell Biol.* 105:3007–3019.

Trybus, K. M., and S. Lowey. 1987*b*. Subunit exchange between smooth muscle myosin filaments. *J. Cell Biol.* 105:3021–3030.

Wang, Y.-L. 1985. Exchange of actin subunits at the leading edge of living fibroblasts: a possible role of treadmilling. *J. Cell Biol.* 101:597–602.

Wang, Y.-L., and D. L. Taylor. 1980. Preparation and characterization of a new molecular cytochemical probe: 5-iodoacetamidofluorescein labeled actin. *J. Histochem.* 28:1198–1206.

Wang, Y.-L., F. Lanni, P. McNeil, B. Ware, and D. L. Taylor. 1982. Mobility of cytoplasmic and membrane associated actin into living cells. *Proc. Natl. Acad. Sci. USA.* 79:4660–4664.

Willingham, M. C., S. S. Yamada, P. J. Bechtel, A. V. Rutherford, and I. H. Pastan. 1981. Ultrastructural immunocytochemical localization of myosin in cultured fibroblastic cells. *J. Histochem. Cytochem.* 29:1289–1301.